

GREEN'S FUNCTIONS OF FILAMENT SOURCES EMBEDDED IN STRATIFIED DIELECTRIC MEDIA

E. A. Soliman [†]

IMEC
Kapeldreef 75, B-3001 Leuven, Belgium

G. A. E. Vandenbosch

K. U. Leuven, ESAT/TELEMIC, Kasteelpark Arenberge 10
B-3001 Leuven, Belgium

Abstract—In this paper a new technique for the evaluation of the Green's functions of filament sources in layered media, is presented. The technique is based on the annihilation of the asymptotic and singular behaviors of a spectral Green's function. The remaining function, after annihilation, is treated using a two levels discrete complex image method (DCIM). The application of the proposed technique, provides a complete analytical expression for the spatial Green's function, in terms of the iterative value of the propagation constant. This expression consists of the annihilating functions and a number of complex images. In order to validate the proposed technique, microstrip lines and slotlines are analyzed and the obtained results are found to agree very well with those obtained using a commercial software.

1. INTRODUCTION

Green's functions are a very important concept in electromagnetics. They are analogous to the impulse response in systems and automatic control theory. Green's functions are the solution of the problem excited with a hypothetical unit source. Mathematically speaking, Green's functions provide the required electromagnetic fields due to a general shape source through a convolution integral. The evaluation

[†] Also with K. U. Leuven, ESAT/TELEMIC, Kasteelpark Arenberge 10, B-3001 Leuven, Belgium

procedure of the Green's functions always starts in the spectral domain. In this domain, several recursive techniques can be employed to calculate the required Green's functions [1–5].

Green's functions are the kernel of the integral equation formulation. Formulating the integral equation in the spatial domain, requires the calculation of the Green's functions in that domain. The spatial domain Green's function is obtained from its spectral equivalent using the inverse Fourier transform operator. Unfortunately, this inverse Fourier transformation results in an integral of the Sommerfeld type [6] whose integrand is a highly oscillatory and slowly decaying function. Consequently, the numerical evaluation of the Sommerfeld integral is very time consuming. Recently, considerable interest has been given to the efficient calculation of the Sommerfeld integrals. A spectral domain Green's function shows an asymptotic behavior at high spectral values. As a first step towards an efficient evaluation of the Sommerfeld integral, this asymptotic behavior should be removed from the spectral Green's function. Most of the techniques presented in the literature are approximating this asymptotic behavior using analytical functions whose inverse Fourier transform are known analytically. The approximating functions are subtracted from the spectral Green's function and their inverses are added analytically in the spatial domain [2, 4, 5, 7].

In addition, the spectral Green's function shows singular behavior due to the existence of poles and branch points located along the real axis. The physical interpretation of a pole is a surface wave mode, which can be considered as an eigen solution to the unloaded dielectric layer structure. The behavior of the poles can also be analytically approximated, subtracted from the spectral functions and their inverse counterparts are analytically added in the spatial domain [2, 4, 5, 7].

The remaining singular behavior is due to the branch points which are associated with the existence of half-spaces in the layer structure under investigation. Most of the techniques presented in the literature avoid these branch points by deforming the Sommerfeld integration path from the real axis to another path in which the branch point singularities do not appear [4, 7]. Since the fast variation in the spectral Green's functions are essentially dominating at large spatial values, the technique presented in [2] provides more accurate Green's functions at high spatial values. In this technique, the branch point singularity is also analytically approximated and subtracted in the spectral domain. Using Fourier transform identities, the inverse Fourier transform is obtained analytically and added. The remaining spectral function along the real axis is a smooth and fast decaying function, which can be integrated numerically [2] over a finite interval.

Alternatively, the remaining spectral function can be integrated more efficiently using the Discrete Complex Image Method, DCIM. The idea of the DCIM was initiated in [8], and developed numerically in [4, 7, 9–11]. It is based on approximating the spectral Green's function using short series of exponentials. This can be achieved by uniformly sampling the spectral function and applying the Generalized Pencil Of Function (GPOF) technique [12], on the samples. The resulting exponentials can be analytically inverse Fourier transformed, using appropriate identities, which results in another series in the spatial domain. A two level DCIM approach is introduced in [13], and used in [14]. It overcomes the difficulties associated with the conventional DCIM approach in selecting the efficient sampling parameters. DCIM can be applied by sampling the remaining spectral function on a modified path if the branch point singularities have not been subtracted [4, 7, 14], or along the real axis if these singularities are subtracted. The latter approach is adopted, for the first time, in this paper.

Section 2 presents the problem under investigation. The evaluation of the Green's functions in the spectral domain is presented in Section 3. In Section 4, the techniques used to transform the Green's functions to the spatial domain are presented. The implementation of the proposed technique is validated by analyzing microstrip lines and slotlines in Section 5. The conclusions are given in Section 6.

2. THE PHYSICAL STRUCTURE

The geometry of the layer structure is shown in Fig. 1. The region consists of a number of flat homogeneous dielectric layers extending infinitely in the lateral xy plane. Each layer, say the j th layer, is characterized by its relative permittivity, ε_{rj} , relative permeability, μ_{rj} , and thickness, d_j . The top-most and the bottom-most layers are either a half-space or a Perfect Electric Conductor (PEC). These layers are referred to as the shielding layers.

Arbitrary number of electric and magnetic filaments are embedded in the layer structure. Electric filaments can be located on any interface except for an interface of a shielding layer representing a PEC. On the other hand, magnetic filaments can only be located on a shielding layer representing a PEC. The filaments extend infinitely along the y -axis. A common phase factor $e^{-j\eta y}$ is assumed and suppressed to all sources and fields, where η is the unknown propagation constant to be determined. The evaluation of η is based on an iterative method [14]. Laterally, the filament source is expressed by a Dirac impulse function. The electromagnetic fields to be observed due to these unit filament sources, i.e., the Green's functions, are the tangential electric field on

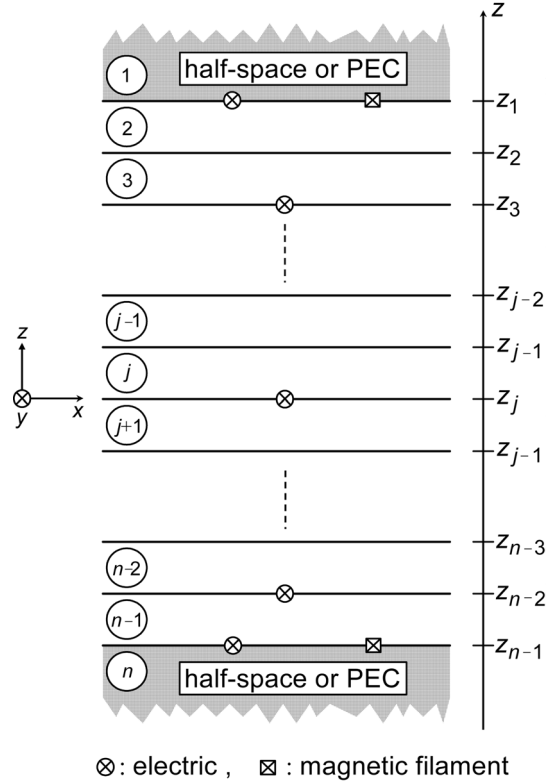


Figure 1. Geometry of a stratified dielectric media carrying filament sources.

the interfaces carrying electric filaments and the tangential magnetic field on the interfaces carrying magnetic filaments. Time harmonic fields with time dependent factor of $e^{-j\omega t}$, where ω is the radial frequency, are assumed and the time factor is suppressed throughout.

3. SPECTRAL DOMAIN GREEN'S FUNCTIONS

In the spectral domain, Maxwell's equations are transformed to the well-known transmission line equations. In these equations, the dependency along the axis of stratification is expressed in terms of two waves propagating in opposite directions and multiplied by unknown expansion coefficients. These coefficients are carrying the dependency along the remaining axes. They can be obtained using the recursive technique presented in [1] and used in [2]. The details of this technique

can be found in [1] and [2], only the main equations are stated in this section. In [1], the authors select e_{ix}^+ , e_{iy}^+ , e_{ix}^- , and e_{iy}^- as the independent field coefficients in the i th layer. In this paper, the coefficients e_{iz}^+ , h_{iz}^+ , e_{iz}^- , and h_{iz}^- are going to be used, which are more convenient in the decomposition of the field into TE-to- z and TM-to- z systems. For the TE system, the coefficients e_{iz}^+ and e_{iz}^- are vanish, and the field components in the i th layer can be written as follows:

$$h_{iz}^{TE} = h_{iz}^{+,TE} \left(e^{-\gamma iz} + \Gamma_i^{TE} e^{\gamma iz} \right) \quad (1)$$

$$e_{ix}^{TE} = \frac{\eta\omega\mu_i}{\beta^2} h_{iz}^{+,TE} \left(e^{-\gamma iz} + \Gamma_i^{TE} e^{\gamma iz} \right) \quad (2)$$

$$e_{iy}^{TE} = \frac{\xi\omega\mu_i}{\beta^2} h_{iz}^{+,TE} \left(e^{-\gamma iz} + \Gamma_i^{TE} e^{\gamma iz} \right) \quad (3)$$

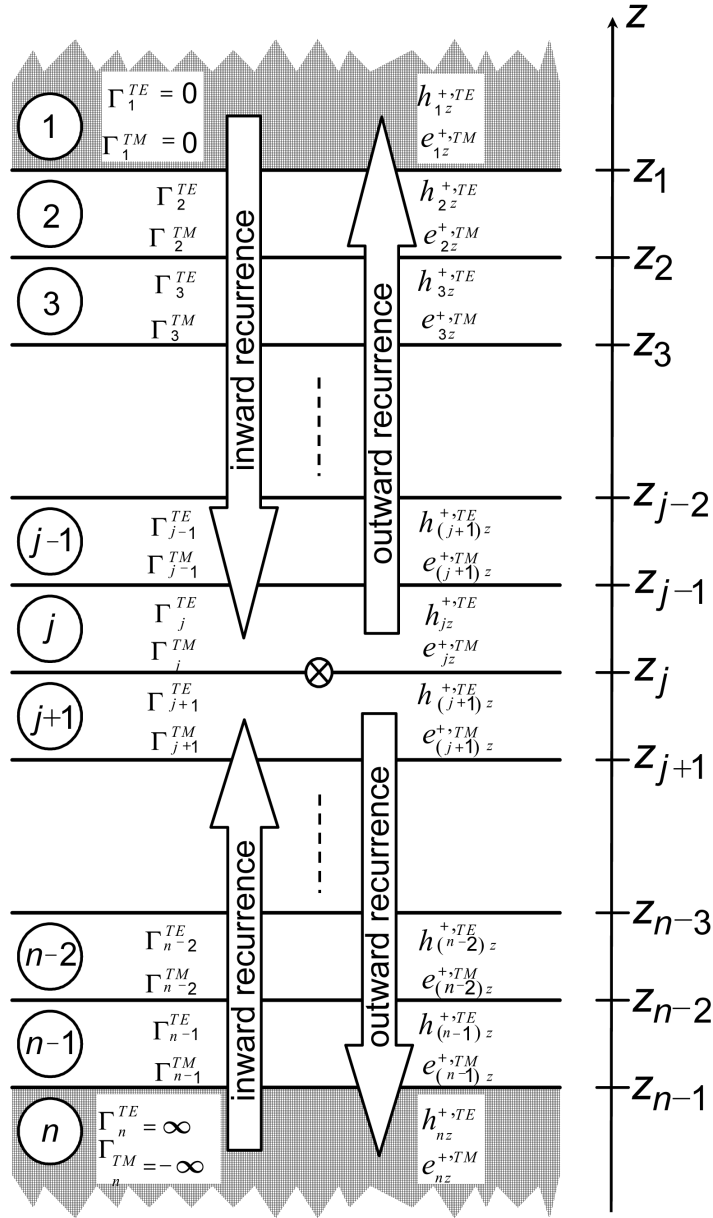
$$h_{ix}^{TE} = \frac{j\xi\gamma_i}{\beta^2} h_{iz}^{+,TE} \left(e^{-\gamma iz} - \Gamma_i^{TE} e^{\gamma iz} \right) \quad (4)$$

$$h_{iy}^{TE} = \frac{j\eta\gamma_i}{\beta^2} h_{iz}^{+,TE} \left(e^{-\gamma iz} - \Gamma_i^{TE} e^{\gamma iz} \right) \quad (5)$$

where ξ is the spectral counterpart of the spatial variable x , $\beta = \sqrt{\xi^2 + \eta^2}$, and $\gamma_i = \sqrt{\beta^2 - \omega^2\mu_i\varepsilon_i}$ is the propagation constant in the i th layer along the direction of stratification. $\Gamma_i^{TE} = h_{iz}^{-,TE}/h_{iz}^{+,TE}$ is defined as the reflection coefficient in the i th layer for the TE system. It is clear from Equations (1)–(5), that all field components of the TE system can be expressed in terms of $h_{iz}^{+,TE}$ and Γ_i^{TE} only. These coefficients can be obtained by applying the recursive technique presented in [1] and shown in Fig. 2. Starting from $\Gamma_i^{TE} = 0$, in the top-most layer, and moving inward while applying the continuity conditions of the tangential fields on the source free interfaces until the j th interface, results in the calculation of all Γ_i^{TE} , where $i < j$, and the j th interface is the interface carrying the source filament. Similarly starting from $\Gamma_n^{TE} = \infty$, in the bottom-most layer, and moving inward, results in the calculation of all Γ_i^{TE} , where $i > j$. This recurrence sequence is referred to as the *inward recurrence*, as shown in Fig. 2. At the j th interface, solving the two equations expressing the field discontinuity, results in the evaluation of $h_{jz}^{+,TE}$ and $h_{(j+1)z}^{+,TE}$. Using these two coefficients and applying an *outward recurrence* sequence, see Fig. 2, towards the top-most and the bottom-most layers, respectively, results in the evaluation of $h_{iz}^{+,TE}$ for all the layers.

Similarly, for the TM system, $h_{iz}^+ = h_{iz}^- = 0$ and the field components can be written as follows:

$$e_{iz}^{TM} = e_{iz}^{+,TM} \left(e^{-\gamma iz} - \Gamma_i^{TM} e^{\gamma iz} \right) \quad (6)$$



\otimes : filament source at the j th interface

Figure 2. Inward and outward recurrence techniques.

$$e_{ix}^{TM} = \frac{j\xi\gamma_i}{\beta^2} e_{iz}^{+,TM} \left(e^{-\gamma_i z} + \Gamma_i^{TM} e^{\gamma_i z} \right) \quad (7)$$

$$e_{iy}^{TM} = \frac{j\eta\gamma_i}{\beta^2} e_{iz}^{+,TM} \left(e^{-\gamma_i z} + \Gamma_i^{TM} e^{\gamma_i z} \right) \quad (8)$$

$$h_{ix}^{TM} = \frac{\eta\omega\varepsilon_i}{\beta^2} e_{iz}^{+,TM} \left(e^{-\gamma_i z} - \Gamma_i^{TM} e^{\gamma_i z} \right) \quad (9)$$

$$h_{iy}^{TM} = -\frac{\xi\omega\varepsilon_i}{\beta^2} e_{iz}^{+,TM} \left(e^{-\gamma_i z} - \Gamma_i^{TM} e^{\gamma_i z} \right) \quad (10)$$

where $\Gamma_i^{TM} = -e_{iz}^{-,TM}/e_{iz}^{+,TM}$ is the reflection coefficient in the i th layer for the TM system. Applying the inward and the outward recurrence sequences, as for the TE case, the coefficients $e_{iz}^{+,TM}$ and Γ_i^{TM} can be calculated for all the layers. The total lateral fields are obtained by recombining the TE and the TM systems [1]:

$$e_{ix} = g_{ij}^{e,ek} k_{jx}^e - j\xi g_{ij}^{e,eq} \left(-j\xi k_{jx}^e - j\eta k_{jy}^e \right) - g_{ij}^{e,mk} k_{jy}^m - j\xi g_{ij}^{e,mq} \left(-j\eta k_{jx}^m + j\xi k_{jy}^m \right) \quad (11)$$

$$e_{iy} = g_{ij}^{e,ek} k_{jy}^e - j\eta g_{ij}^{e,eq} \left(-j\xi k_{jx}^e - j\eta k_{jy}^e \right) + g_{ij}^{e,mk} k_{jx}^m - j\eta g_{ij}^{e,mq} \left(-j\eta k_{jx}^m + j\xi k_{jy}^m \right) \quad (12)$$

$$h_{ix} = -g_{ij}^{h,ek} k_{jy}^e - j\xi g_{ij}^{h,eq} \left(-j\eta k_{jx}^e + j\xi k_{jy}^e \right) + g_{ij}^{h,mk} k_{jx}^m - j\xi g_{ij}^{h,mq} \left(-j\xi k_{jx}^m - j\eta k_{jy}^m \right) \quad (13)$$

$$h_{iy} = g_{ij}^{h,ek} k_{jx}^e - j\eta g_{ij}^{h,eq} \left(-j\eta k_{jx}^e + j\xi k_{jy}^e \right) + g_{ij}^{h,mk} k_{jy}^m - j\eta g_{ij}^{h,mq} \left(-j\xi k_{jx}^m - j\eta k_{jy}^m \right) \quad (14)$$

where k_{jx}^e and k_{jy}^e are the x - and y -component of the electric filament current source located at the j th interface, while k_{jx}^m and k_{jy}^m are the magnetic current components. Practically, the j th interface can carry either electric or magnetic filaments. However, it is assumed that both kinds of sources are present in order to mathematically treat both cases simultaneously. The function g_{ij} is the spectral domain Green's function representing a field observed on the i th interface due to a unit filament source located on the j th interface. The superscript of any spectral Green's function in Equations (11)–(14) consists of three letters. The first letter indicates the type of field to be observed, e for electric and m for magnetic field. The second and third letters are related to the source. The second letter indicates the type of the current, e for electric and m for magnetic. The third letter is set to k

if the current source is directly used, while it is set to q if the charge derived from the current source is used.

It is worth mentioning here that all Green's functions in Equations (11)–(14) are depending on β , and independent on ξ separately. The field components in the spatial domain can be obtained by performing inverse Fourier transform operations on Equations (11)–(14). The resulting spatial domain field components are related to the spatial current components and spatial Green's functions through convolution integrals. It is our objective in the following section to evaluate the spatial equivalent of the spectral Green's functions obtained in this section.

4. SPATIAL DOMAIN GREEN'S FUNCTIONS

After evaluating the spectral Green's functions, an inverse Fourier transform is performed in order to transform them to the spatial domain. Making use of the fact that the spectral Green's functions are dependent on β , and independent on ξ separately, the inverse Fourier transform can be written as follows:

$$FT^{-1}(g(\xi)) = G(x) = \frac{1}{\pi} \int_0^{\infty} g\left(\sqrt{\xi^2 + \eta^2}\right) \cos(\xi x) d\xi \quad (15)$$

where G and g are the spatial and spectral domain Green's functions, respectively. FT^{-1} is the inverse Fourier transform operator. The integral in (15) is a typical Sommerfeld cosine integral, which is quite time consuming to be evaluated numerically owing to its highly oscillating and slowly decaying integrands. Several authors have given their interest towards the efficient evaluation of Sommerfeld integrals. The technique presented here is a combination between an extended version from the technique in [2] and a modified version of the technique presented in [14]. Consequently, it is highly recommended to consult these works.

4.1. Annihilation of the Asymptotic and Singular Behaviors

The technique presented in [2], is based on subtracting a number of analytical, annihilating, functions from a spectral domain Green's function. These functions are representing the asymptotic and the singular behaviors of the function. The asymptotic functions are approximating the Green's function at high spectral values. The singular functions are approximating the Green's function around a pole or a branch point. The annihilating functions are selected such

Table 1. Fourier transform pairs for the annihilating functions.

category	Spectral Domain	spatial Domain
Asymptotes	$e^{-\beta\Delta}$	$\frac{\Delta\eta}{\pi\sqrt{x^2+\Delta^2}}K_1(\eta\sqrt{x^2+\Delta^2})$
	$\frac{1-e^{-\beta t}}{\beta}e^{-\beta\Delta}$	$\frac{1}{\pi}\left[K_0(\eta\sqrt{x^2+\Delta^2})-K_0(\eta\sqrt{x^2+(t+\Delta)^2})\right]$
Branch points	$\sqrt{\beta^2-K^2}-\beta+\frac{K^2}{2\sqrt{\beta^2+K^2}}$	$\frac{\sqrt{\eta^2-K^2}}{\pi x}K_1(\sqrt{\eta^2-K^2}x)-\frac{\eta}{\pi x}K_1(\eta x)+\frac{K^2}{2\pi}K_0(\sqrt{\eta^2+K^2}x)$
Branch points close to poles	$\frac{1}{\sqrt{\beta^2-K^2}}-\frac{P}{\beta^2-K^2}-\frac{1}{\sqrt{\beta^2+K^2}}-\frac{P}{\beta^2+K^2}$	$\frac{1}{\pi}K_0(\sqrt{\eta^2-K^2}x)-\frac{P}{2\sqrt{\eta^2-K^2}}e^{-\sqrt{\eta^2-K^2}x}-\frac{1}{\pi}K_0(\sqrt{\eta^2+K^2}x)+\frac{P}{2\sqrt{\eta^2+K^2}}e^{-\sqrt{\eta^2+K^2}x}$
Poles	$\frac{1}{\beta^2-P^2}-\frac{1}{\beta^2+P^2}$	$\frac{1}{2\sqrt{\eta^2-P^2}}e^{-\sqrt{\eta^2-P^2}x}-\frac{1}{2\sqrt{\eta^2+P^2}}e^{-\sqrt{\eta^2+P^2}x}$

that their inverse Fourier transforms are known analytically. In [2], the spatial counterparts of the annihilating functions are given for the case of dipole sources. For the filament source problem under investigation, the same annihilating functions are used in the spectral domain, while their spatial counterparts are different due to the fact that different inverse Fourier transform operator is used.

Table 1 lists the spectral and the spatial pairs of each annihilating function. In this table, Δ is the z -separation between the source and the observation point, $t = 1/\kappa_m$ and $\kappa_m = \kappa_0\sqrt{\varepsilon_{r,m}}$ is the maximum propagation constant in the layer structure, $\kappa_0 = \omega\sqrt{\mu_0\varepsilon_0}$ is the free-space propagation constant, and $\varepsilon_{r,m}$ is the maximum relative permittivity in the layer structure. P and K are the spectral points, along the real axis of β , representing a pole and a branch point, respectively. K_n is the modified Bessel function of the second kind and of the n th order. In Table 1, the terms used to annihilate the asymptotes are those representing the direct term between the source and the observer. For most of the layer structures, these terms are the dominant terms. However, for layer structures containing very thin film, like in the multichip module-deposition (MCM-D) technology [14], the indirect terms resulting from the multiple reflections may become significant. Consequently, for these special cases, the annihilation of the direct terms only, leave the function with residual asymptotes. These residual asymptotes are treated numerically in this paper via the application of a two level discrete complex image method, DCIM.

In order to demonstrate the annihilation procedure, an electric filament located on top of an alumina substrate, with $\varepsilon_r = 9.9$

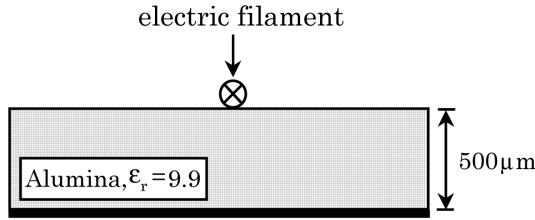


Figure 3. Electric filament source on top of an alumina substrate backed by a PEC.

and thickness of $500 \mu\text{m}$, backed by a PEC plane is considered, see Fig. 3. The integral equation formulation of this problem, requires the evaluation of two Green's functions, namely $g_{11}^{e,ek}$ and $g_{11}^{e,eq}$ which correspond to the electric field observed on the air-dielectric interface due to the current and charge, respectively, of the electric filament source located on the same interface. As a representative example, only $g_{11}^{e,eq}$ will be treated, it will be referred to as g throughout. The other function can be treated in a similar way. Fig. 4 shows the function g versus β/κ_0 , calculated at frequency $f = 5 \text{ GHz}$. The figure clearly shows both the asymptotic and the singular behaviors of the Green's function. Subtracting the annihilating functions listed in the second column of Table 1, results in the *modified* Green's function, g_{mo} , which is plotted in Fig. 5. It is clear that the modified function is free from any asymptotic or singular behaviors. It is suitable to be treated numerically along the real axis of β using DCIM.

4.2. Discrete Complex Image Method (DCIM)

In [2], the modified function is inverted numerically over a finite interval. In this paper, the two level discrete complex image method, DCIM, introduced in [13] is applied on the modified function. Unlike [14], the application of the DCIM technique is carried out along the real axis of β , in both the first and second levels. This selection is a consequence of the complete annihilation of the singularities along the real axis.

The first and second levels are defined in the spectrum $\beta_2 \rightarrow \beta_1$ and $\kappa_0 \rightarrow \beta_2$, respectively, where κ_0 is the free-space propagation constant. The values of β_1 and β_2 are not strictly specified. Numerical investigations on several layer structures, have shown that $\beta_1 = 100 \kappa_0$ is enough to extract any residual asymptotic behavior of the spectral Green's function in the first level. β_2 is selected such that it is higher

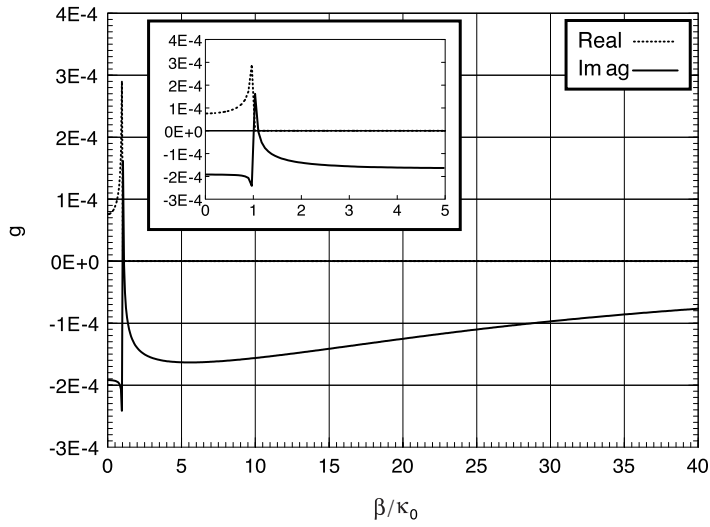


Figure 4. Spectral charge Green's function for the electric filament source of Fig. 3, $f = 5$ GHz.

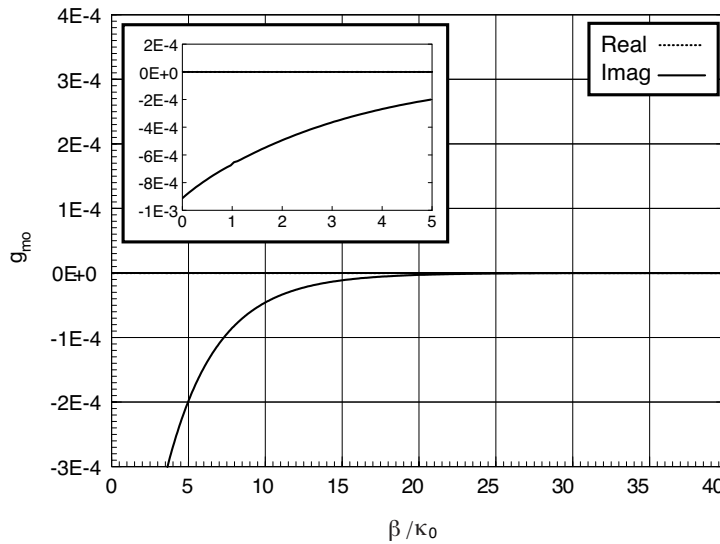


Figure 5. Modified spectral charge Green's function after subtracting the annihilating functions.

than κ_m , where κ_m is the maximum total propagation constant in the layer structure under investigation. This selection is based on the fact that any residual singular behavior, which could not be annihilated perfectly, should be located in the spectrum below κ_m . The function in the first level is sampled with low sampling rate, while in the second level, higher sampling rate is required to pick-up the relatively faster variation of the function.

The parametric equation of the first level, according to which the samples are taken, can be written as follows:

$$\beta = \beta_2 + (\beta_1 - \beta_2)t, \quad t : 0 \rightarrow 1 \quad (16)$$

Using GPOF [12], the spectral domain Green's function in the first level can be written as follows:

$$g_1 = \sum_{i=1}^{N_1} a_{1i} e^{\alpha_{1i} t} \sum_{i=1}^{N_1} a_{1i} e^{\alpha_{1i}(\beta - \beta_2)/(\beta_1 - \beta_2)} \quad (17)$$

where g_1 is the spectral Green's function in the first level, N_1 is the number of exponentials required to approximate the function in the first level, a_{1i} and α_{1i} are the complex residue and exponent of the i th exponential term, respectively. The approximated function, g_1 , matches the original function in the first level, $\beta : \beta_2 \rightarrow \beta_1$, where the function shows an asymptotic behavior. Although the Green's function asymptote associated with the direct term has been removed, the investigation of the function in the first level is performed in order to extract the asymptote associated with the indirect terms appearing in thin film layer structures. The extrapolation of the function g_1 in the second level does not match the original function, g . Another DCIM procedure should be applied in the second level to approximate the difference between the original function, g , and the extrapolation of g_1 [13]. The parametric equation of the second level is:

$$\beta = \kappa_0 + (\beta_2 - \kappa_0)t, \quad t : 0 \rightarrow 1 \quad (18)$$

Applying GPOF on the difference: $g_2 = g - g_1$, allows one to write:

$$g_2 = \sum_{i=1}^{N_2} a_{2i} e^{\alpha_{2i} t} = \sum_{i=1}^{N_2} a_{2i} e^{\alpha_{2i}(\beta - \kappa_0)/(\beta_2 - \kappa_0)} \quad (19)$$

where N_2 is the number of exponentials required to approximate the difference function in the second level, a_{2i} and α_{2i} are the complex residue and exponent of the i th exponential term, respectively. Being the difference between the original and the approximated function

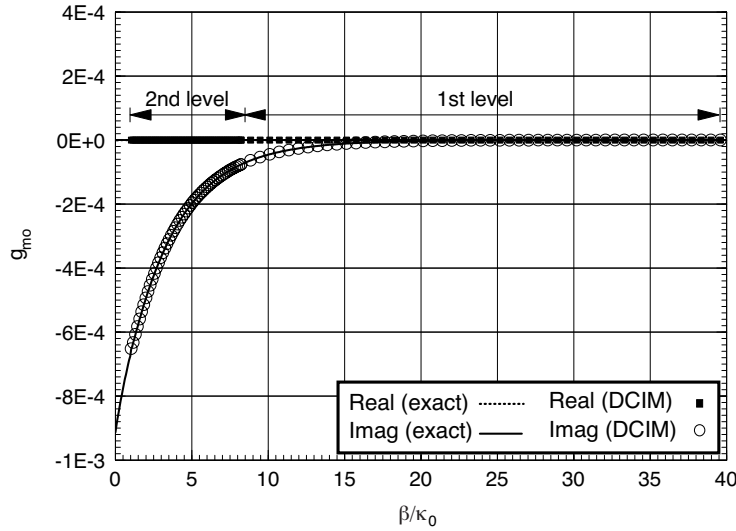


Figure 6. Exact and DCIM approximation of the modified spectral charge Green's function.

in the first level, the extrapolation of the approximated function, g_2 , should vanish in the first level. Hence, over all the investigated spectrum, $\beta : \kappa_0 \rightarrow \beta_1$, the modified spectral Green's function can be approximated as follows:

$$g_{mo}(\beta) = g_1 + g_2 = \sum_{i=1}^{N_1} a_{1i} e^{\alpha_{1i}(\beta-\beta_2)/(\beta_1-\beta_2)} + \sum_{i=1}^{N_2} a_{2i} e^{\alpha_{2i}(\beta-\kappa_0)/(\beta_2-\kappa_0)} \quad (20)$$

The exact and the two levels DCIM approximation of the modified charge function g_{mo} , of the example in Fig. 3, are plotted in Fig. 6. The figure shows very good approximation for the modified function in both the first and second levels. Using a Fourier transform identity [15], the modified spectral Green's function in Equation (20) can be written in the spatial domain as follows:

$$G_{mo}(x) = \frac{\eta}{\pi(\beta_1 - \beta_2)} \sum_{i=1}^{N_1} \pm \frac{\alpha_{1i} \alpha_{1i}}{\rho_{1i}} K_1(\eta \rho_{1i}) e^{\frac{\alpha_{1i} \beta_2}{\beta_1 - \beta_2}} + \frac{\eta}{\pi(\beta_2 - \kappa_0)} \sum_{i=1}^{N_2} \pm \frac{\alpha_{2i} \alpha_{2i}}{\rho_{2i}} K_1(\eta \rho_{2i}) e^{\frac{\alpha_{2i} \kappa_0}{\beta_2 - \kappa_0}} \quad (21)$$

where $\rho_{1i} = \sqrt{(\alpha_{1i}/(\beta_1 - \beta_2))^2 + x^2}$ and $\rho_{2i} = \sqrt{(\alpha_{2i}/(\beta_2 - \kappa_0))^2 + x^2}$.

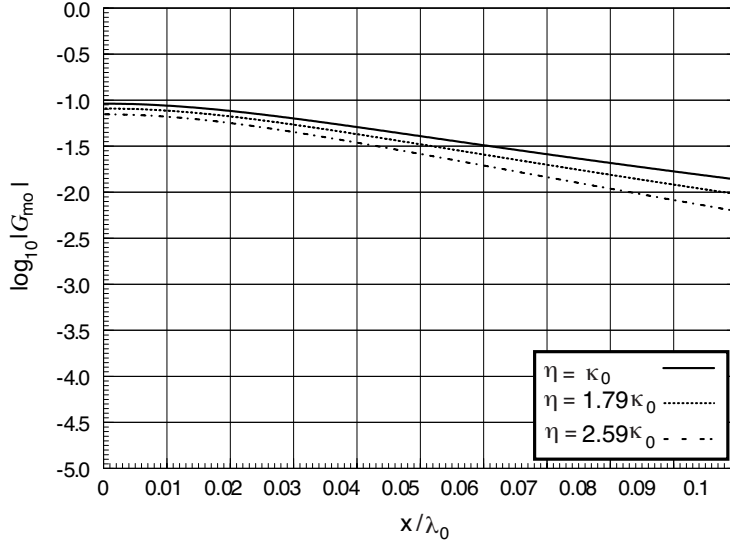


Figure 7. Modified spatial charge Green's function.

The + and the – signs are used if $\text{Re}(\alpha_i) > 0$ and $\text{Re}(\alpha_i) < 0$, respectively. Equation (21) shows that we can look at the modified spatial Green's function G_{mo} as constructed from the contribution of several sources, *images*, located at complex distances ρ . Fig. 7 shows the modified spatial Green's function versus x/λ_0 , where λ_0 is the free-space wavelength. Three values for the iterative propagation constant η are used: κ_0 , $1.79\kappa_0$, and $2.59\kappa_0$. The last value of η is the propagation constant of a microstrip line of width $500\mu\text{m}$ located on the same interface as the filament source in Fig. 3.

4.3. Recombination Procedure

The last step towards obtaining the spatial Green's function is to add the spatial equivalent of the annihilating functions to the spatial modified Green's function of Fig. 7. The spectral annihilating functions have been subtracted in Section 4.1. The third column of Table 1 lists these functions in the spatial domain. Obviously, the subtracted and added functions in the second and third column, respectively, of Table 1 should be multiplied by suitable coefficients [2]. After recombination, the required spatial Green's function is obtained and plotted in Fig. 8. The same three values of η are used: κ_0 , $1.79\kappa_0$ and $2.59\kappa_0$.

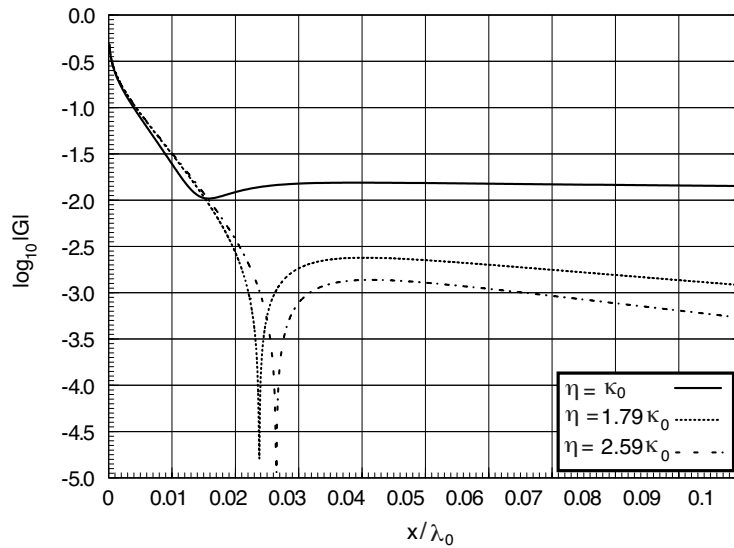


Figure 8. Spatial charge Green's function.

5. VALIDATION RESULTS

In this section, two types of planar guiding structures are analyzed, namely: microstrip lines and slotlines. The analysis of these guiding structures is carried out using a method of moment (MoM) formulation similar to that presented in [14]. The core of this MoM uses the spatial domain Green's functions calculated via the proposed approach in this paper. The analysis of the structures under investigation is carried out using Agilent-Momentum [16] as well. Comparison between ours and Momentum's results is performed.

5.1. Microstrip Lines

The microstrip line studied in this sub-section is built on an Alumina substrate with dielectric constant of $\epsilon_r = 9.9$, and thickness of $500 \mu\text{m}$. The substrate is backed by a perfect electric conductor (PEC) plate. On top of the substrate a thin film of BenzoCycloButene (BCB) is deposited. The dielectric constant of this layer is 2.7, and its thickness is d . Above the BCB film, a microstrip line made of copper ($\sigma = 58 \times 10^6 \text{ 1}/\Omega\text{m}$) with width of $500 \mu\text{m}$ and thickness of $2 \mu\text{m}$, is placed. Another thin film of BCB with thickness of $10 \mu\text{m}$, is placed on top of the microstrip line. The deposition of the BCB thin films is a typical feature of the MCM-D technology [14]. These films are used

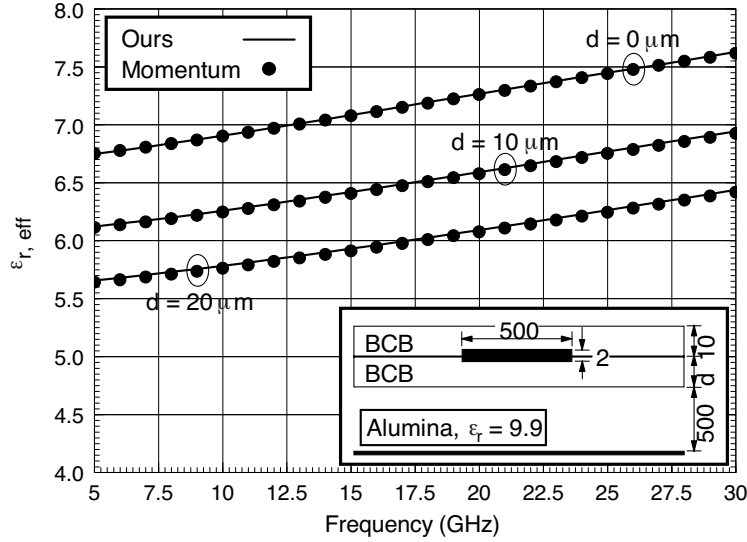


Figure 9. Effective dielectric constant versus frequency for the microstrip line using 3 uniform segments along the width (all dimensions are in μm).

to isolate the layers of interconnects of the MCM.

The effective dielectric constant versus frequency obtained using both our solver and Momentum is plotted in Fig. 9. The cross section of the microstrip line is also shown in Fig. 9. Three uniform segments are used to model the width of the microstrip line. The thickness of the bottom BCB film takes the values: 0, 10 μm , and 20 μm . Very good agreement between our results and those of Momentum is observed. This agreement validates indirectly the proposed technique for calculating the spatial domain Green's functions.

It is clear from the figure that as the thickness of the bottom BCB film increases, the effective dielectric constant of the microstrip line decreases. This means that the phase velocity increases and the propagation delay decreases. Consequently, we can conclude that microstrip lines in the MCM-D technology are performing better than those fabricated with the conventional technology. The thickness of the top BCB film is found to have a negligible effect on the effective dielectric constant of the microstrip line. This comes from the fact the most of the power is concentrated in the high dielectric constant substrate below the microstrip line. Hence, the thickness of the top BCB film is held constant at 10 μm .

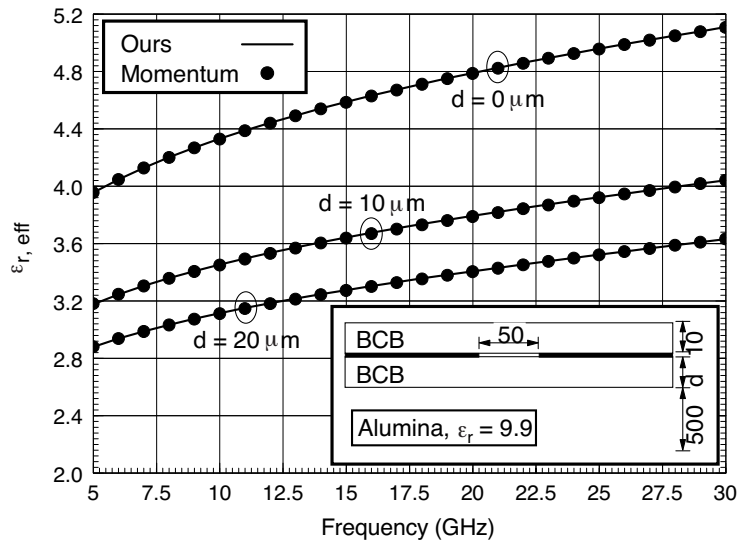


Figure 10. Effective dielectric constant versus frequency for the slotline using 3 uniform segments along the width (all dimensions are in μm).

5.2. Slotlines

In this subsection, a slotline of $50\ \mu\text{m}$ width is studied. The slotline is embedded in the same dielectric layer structure used for the microstrip line. The PEC plate is removed from the bottom of the substrate and placed between the two BCB films. The slotline is etched in the PEC plate. The effective dielectric constant of the slotline, as calculated using both our solver and Momentum, is plotted versus frequency in Fig. 10. The figure shows also a cross-section for the slotline. Three uniform segments are used to model the width of the slotline. Fig. 10 shows the results for three different values for the thickness of the bottom BCB film: 0, $10\ \mu\text{m}$, and $20\ \mu\text{m}$. Very good agreement is observed between our results and those of Momentum. Increasing the thickness of the bottom BCB film results in decreasing the effective dielectric constant. This is attributed to the decrease in the value of the shunt capacitance, per unit length, of the equivalent circuit of the slotline. Consequently, the phase velocity increases and the propagation delay decreases. It has been found that the thickness of the top BCB film has a negligible effect on the propagation characteristic because of the fact that most of the power is concentrated below the slotline. The Green's functions derived in the previous

sections are used in the calculation of the propagation characteristic of the slotline. Consequently, the agreement between our solver and Momentum validates the theory and the implementation of the Green's functions.

6. CONCLUSIONS

In this paper, a modified technique for the evaluation of the Green's functions of filament sources in layered media is presented. It generalizes the technique in [2] to be suitable for applications containing wire-like sources. Moreover, it also generalizes the two levels DCIM technique presented in [13] to the problem under investigation. This generalized two levels DCIM is used to replace the conventional numerical integral used in [2] for inverting the modified spectral Green's function. The mixture of the two generalized techniques allows complete analytical representation for spatial Green's functions of filament sources embedded in layer structure containing thin films.

Since the solution procedure of the planar guiding structure problems is iterative and requiring the evaluation of a new set of spatial Green's functions at each iteration. The technique presented in this paper is found to be numerically efficient. This comes from the fact that after the first iteration, the spectral Green's functions are expressed as number of analytical functions: the annihilating functions, and number of complex images. Consequently, the spatial domain Green's functions are also expressed analytically as a function of the iterative value of the propagation constant. Then for the next iterations, the new set of spatial Green's functions is obtained by simple substitution in the analytical expressions with a new value of the iterative variable.

The technique presented in this paper provides higher accuracy than that presented in [14], specially at large spatial distances. This is a consequence of the careful treatment of the singular behaviors whose contributions are known to dominate at these distances. The accuracy of proposed technique is validated by analyzing a number of microstrip lines and slotlines. Our results are compared with those obtained using a commercial software. Very good agreement is observed.

REFERENCES

1. Vandenbosch, G. A. E. and A. R. Van de Capelle, "Mixed-potential integral expression formulation of the electric field in a stratified dielectric medium — Application to the case of a probe

- current source," *IEEE Trans. Antennas Propagat.*, Vol. 40, 806–817, 1992.
2. Demuynck, F. J., G. A. E. Vandenbosch, and A. R. Van de Capelle, "The expansion wave concept — Part I: Efficient calculation of the spatial Green's functions in a stratified dielectric medium," *IEEE Trans. Antennas Propagat.*, Vol. 46, 397–406, 1998.
 3. Michalski, K. A. and D. Zheng, "Electromagnetic scattering and radiation by surfaces of arbitrary shape in layered media, Part I: Theory," *IEEE Trans. Antennas Propagat.*, Vol. 38, 335–344, 1990.
 4. Dural, G. and M. I. Aksun, "Closed-form Green's function for general sources and stratified media," *IEEE Trans. Microwave Theory Tech.*, Vol. 43, 1545–1552, 1995.
 5. Hsu, C.-I. G., R. F. Harrington, K. A. Michaliski, and D. Zheng, "Analysis of multiconductor transmission lines of arbitrary cross section in multilayered uniaxial media," *IEEE Trans. Microwave Theory Tech.*, Vol. 41, 70–78, 1993.
 6. Sommerfeld, A., *Partial Differential Equations in Physics*, Academic, New York, 1949.
 7. Chow, Y. L., J. J. Yang, D. G. Fang, and G. E. Howard, "A closed-form spatial Green's function for the thick microstrip substrate," *IEEE Trans. Microwave Theory Tech.*, Vol. 39, 588–592, 1991.
 8. Mohsen, A., "On the evaluation of Sommerfeld integrals," *IEE Proc. Pt. H.*, Vol. 129, 177–182, 1982.
 9. Mahmoud, S. F. and A. Mohsen, "Assessment of image theory for field evaluation over a multi-layer earth," *IEEE Trans. Antennas Propagat.*, Vol. 33, 1054–1058, 1985.
 10. Yang, J. J., Y. L. Chow, and D. G. Fang, "Discrete complex images of a three-dimensional dipole above and within a lossy ground," *IEE Proc. Pt. H.*, Vol. 138, 319–326, 1991.
 11. Chow, Y. L., J. J. Yang, and G. E. Howard, "Complex images for electrostatic field computation in multilayered media," *IEEE Trans. Microwave Theory Tech.*, Vol. 39, 1120–1125, 1991.
 12. Hua, Y. and T. K. Sarker, "Generalized pencil-of-function method for extracting poles of an EM system from its transient response," *IEEE Trans. Antennas Propagat.*, Vol. 37, 229–234, 1989.
 13. Aksun, M. I., "A robust approach for the derivation of closed-form Green's functions," *IEEE Trans. Microwave Theory Tech.*, Vol. 44, 651–658, 1996.
 14. Soliman, E. A., P. Pieters, E. Beyne, and G. A. E. Vandenbosch,

- “Numerically efficient spatial domain moment method for multislotted transmission lines in layered media — Application to multislotted lines in MCM-D technology,” *IEEE Trans. Microwave Theory Tech.*, Vol. 47, 1782–1787, 1999.
15. Gradshteyn, I. S. and I. M. Ryzhik, *Table of Integrals, Series and Products*, Academic Press, 1980.
 16. *Momentum*, version 4.8, Agilent Technologies, 2003.